



Synthesis and application of ZnO-MgO-NiO@Stearicamide mixed oxide for removal of ciprofloxacin and ampicillin from aqueous solution

Olamide A. Olalekan^a, Abisola J. Campbell^a, Adewale Adewuyi^{a,*}, Woei Jye Lau^{b,c}, Olalere G. Adeyemi^a

^a Department of Chemical Sciences, Faculty of Natural Sciences, Redeemer's University, Ede, Osun State, Nigeria

^b School of Chemical and Energy Engineering, Universiti Teknologi Malaysia, 81310 Skudai, Johor, Malaysia

^c Department of Civil Engineering, Apadana Institute of Higher Education, Shiraz, Iran

ARTICLE INFO

Keywords:

Adsorption
Ampicillin
Antibiotics
Ciprofloxacin
Metal mixed oxide

ABSTRACT

The presence of ciprofloxacin (CIP) and ampicillin (AMP) as emerging contaminant in water is a serious global challenge requiring affordable and sustainable solution. In response to this, this study prepared a mixed metal oxide, zinc oxide (ZnO)-magnesium oxide (MgO)-nickel oxide (NiO)@stearicamide for the removal of CIP and AMP from aqueous solution. The properties of ZnO-MgO-NiO@Stearicamide were confirmed with several analyses including Fourier transformed infrared spectroscopy (FTIR), Brunauer-Emmett-Teller (BET), transmission electron microscopy (TEM), X-ray diffraction (XRD) and energy-dispersive X-ray spectroscopy (EDX). ZnO-MgO-NiO@Stearicamide has a BET surface area of $13.50 \text{ m}^2 \text{ g}^{-1}$ and an average particle size of 12.50 nm. The sorption of CIP and AMP from solution by ZnO-MgO-NiO@Stearicamide showed a removal of 83.87 % and 81.10 %, respectively in a process that can be described by the Langmuir isotherm and electrostatic interaction. The sorption process has enthalpy (ΔH), entropy (ΔS) and free energy change (ΔG) which suggests the process to be spontaneous and exothermic. It is also found that synthesized metal mixed oxide could maintain a regeneration capacity that is > 80 % even after 11th regeneration cycle. The experimental findings indicate that the self-synthesized ZnO-NiO-MgO@Stearicamide is a potential material to treat CIP- and AMP-contaminated water source.

1. Introduction

Contamination of environmental water systems by antibiotics has emerged as serious environmental problem [1]. Antibiotics contamination has been reported in surface water, municipal sewage, groundwater, and drinking water [2–5] which poses a serious threat to human health because of the toxicity of the resulting side products generated from their persistence in the environment. Their presence in the environment has also led to the emergence of drug-resistant strains of pathogenic organisms in water which is a disaster to the efficacy of these antibiotics in disease treatment [6,7]. An illustration indicating how these antibiotics get into environmental water system is shown in Fig. 1.

Ciprofloxacin (CIP) and ampicillin (AMP) are two antibiotics that are frequently reported in environmental water system. Therefore, it is important to develop mechanism for their removal in water systems. Although several methods have been reported in times past [8–12], some of these methods suffer from shortcomings like incomplete

removal, generation of side products, and being expensive.

Among the known methods reported for the purification of water contaminated with CIP and AMP, adsorption remains a promising method that can achieve this purpose [13]. Adsorption is promising because the surface of adsorbents can be easily modified to target specific contaminants in solution [14]. Moreover, adsorbents can be easily prepared or sourced from cheap materials that are readily available to achieve optimum result. Several types of adsorbents have been prepared overtime for the purification of contaminated water, many of which have shortcomings like poor regeneration capacity, poor selectivity, and sometimes expensive. To address these shortcomings, the work proposes the use of mixed metal oxides which are new generation of materials receiving attention as adsorbents for water purification due to their small size, large surface area, and ease of regeneration for further use [15–17].

Metal mixed oxides are combination of transition metals that have found applications in various areas of research such as in chemical

* Corresponding author.

E-mail address: walex62@yahoo.com (A. Adewuyi).

reaction processes and biologically induced reactions [18–21]. Literature also reveals that mixed oxides also exhibit adsorptive properties when used as catalyst [22]. While most researchers focus on the catalytic applications there are limited studies on their use as adsorbents.

This study therefore aimed at preparing cheap and efficient metal mixed oxide for the purification of water contaminated with antibiotics (CIP and AMP). To achieve this, mixed oxides, i.e., zinc oxide (ZnO),

nickel oxide (NiO) and magnesium oxide (MgO) were considered. ZnO is an *n*-type semiconductor while NiO is a *p*-type semiconductor. MgO has an excellent thermodynamic stability which makes it a suitable component of the proposed mixed oxide (ZnO-MgO-NiO). The structural benefits of the oxides suggest them as possible materials for adsorption of micropollutants in water. In fact, MgO has been previously shown as adsorbents for toxic chemical [23]. ZnO was reported as an excellent

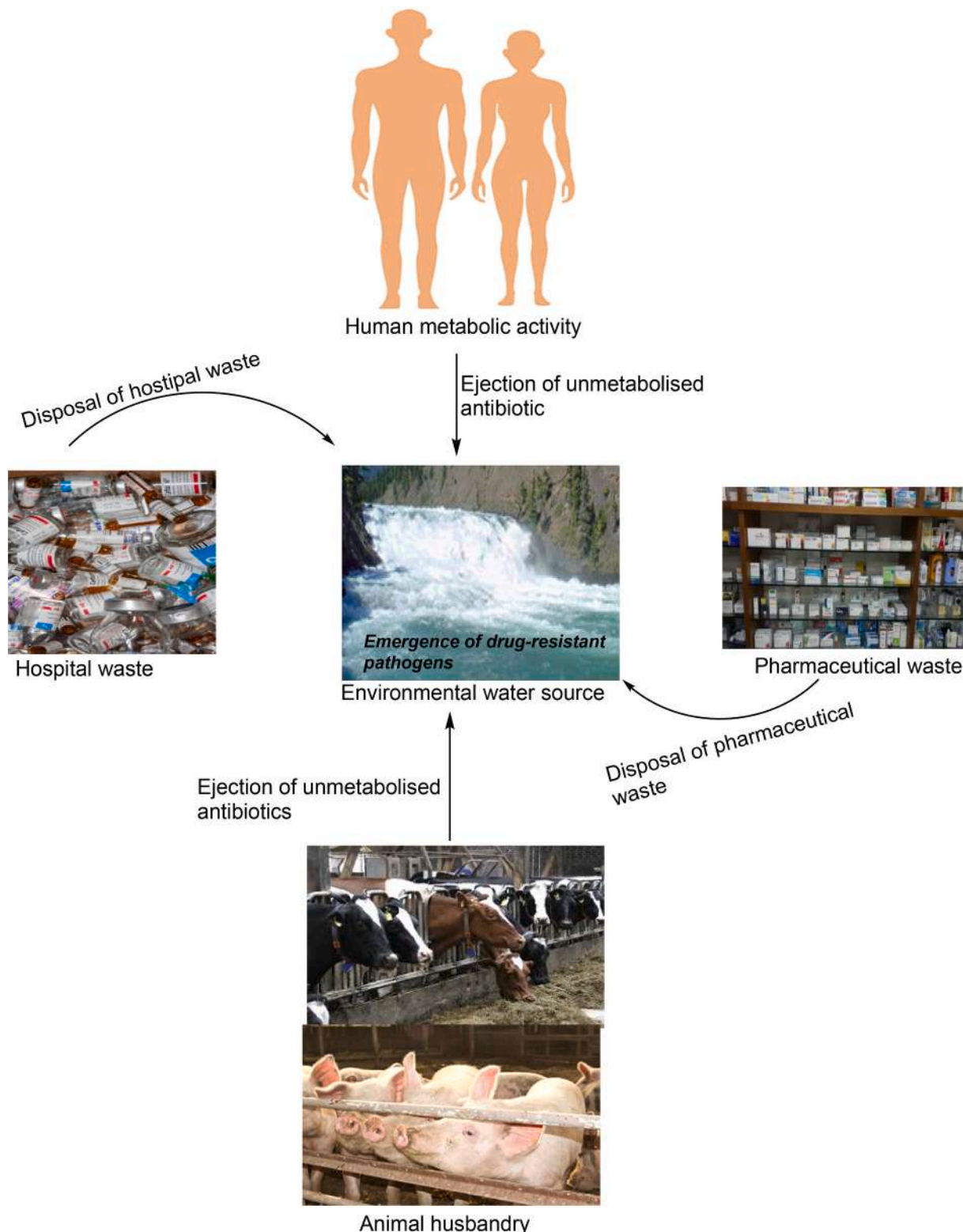


Fig. 1. Antibiotics in environmental water system.

adsorbent for organic dyes in solution but its use as adsorbent for CIP and AMP is rarely reported [24]. The fact that previous study showed that ZnO expressed high selectivity and adsorption capacity towards cationic and anionic dyes in solution [25] is an indication or probability that it may be useful for the removal of CIP and AMP from solution. The surface of NiO has been described to have charges and dipole moment which influences its adsorption property [26] while its adsorption kinetics and model towards rhodamine B in solution has been reported [27]. NiO may be considered as a promising adsorbent because of its magnetic and chemical properties [28]. Interestingly, mixing these oxides (i.e., ZnO, NiO and MgO) can improve the electronic structure, transport and surface properties of the resulting mixed oxides formed [29].

It must be pointed out that one disadvantage to the use of metal mixed oxide as adsorbent for water purification is their poor recovery from solution after treatment due to their small size [30]. Several studies have reported the use of large organic molecules such metal organic-framework [31,32] to overcome this challenge. However, the cost of synthesizing these organic molecules is high which makes the overall material expensive.

The current study considers the use of long chain fatty amides such as stearic amide to modify the particle size of mixed oxide of Zn, Mg and Ni in order to improve their recovery from solution after being used as adsorbent. Therefore, this present work synthesized ZnO-MgO-NiO@stearicamide as adsorbent for the removal of CIP and AMP from contaminated water system. To the best of our knowledge, there is limited information on the use of ZnO-MgO-NiO@stearicamide as adsorbent for the removal of CIP and AMP from aqueous solution.

2. Materials and methods

2.1. Materials

Zinc (II) chloride hexahydrate ($\text{ZnCl}_2 \cdot 6\text{H}_2\text{O}$), nickel (II) chloride hexahydrate ($\text{NiCl}_2 \cdot 6\text{H}_2\text{O}$), magnesium dichloride hexahydrate ($\text{MgCl}_2 \cdot 6\text{H}_2\text{O}$), stearic amide ($\text{C}_{18}\text{H}_{37}\text{NO}$), sodium hydroxide (NaOH), oleic acid, ethanol, and hydrochloric acid (HCl) were purchased from Aldrich Chemical Co., England. Ciprofloxacin ($\text{C}_{17}\text{H}_{18}\text{FN}_3\text{O}_3$) and ampicillin ($\text{C}_{16}\text{H}_{19}\text{N}_3\text{O}_4\text{S}$) were purchased from a pharmacy store in Ede, Osun state, Nigeria.

2.2. Synthesis of ZnO-MgO-NiO@Stearicamide particles

ZnO-MgO-NiO particles were synthesized by mixing solutions of $\text{ZnCl}_2 \cdot 6\text{H}_2\text{O}$ (0.2 M), $\text{MgCl}_2 \cdot 6\text{H}_2\text{O}$ (0.2 M) and $\text{NiCl}_2 \cdot 6\text{H}_2\text{O}$ (0.2 M) in ratio 1:1:1 in a 1-L beaker. The mixture was stirred continuously for 40 min after which oleic acid (10 mL) was added as a capping agent to control the growth of the mixed oxide particles while the stirring continued for another 1 h raising the temperature gradually to 80 °C. The pH of the mixture was brought to 12 by dropwise addition of NaOH (2 M) solution to precipitate the ZnO-MgO-NiO particles out of solution while keeping the temperature at 80 °C. The mixture was then cooled to room temperature, filtered and the residue washed several times with deionized water until a neutral pH was obtained. The residue was transferred into a crucible and kept in the furnace at 550 °C for 20 h. The ZnO-MgO-NiO particles (10 g) were then poured into 250-mL round bottom flask (placed in an oil bath) containing 150-mL stearic amide solution (5 mg L⁻¹). The reaction mixture was continuously stirred for 3 h at 80 °C followed by cooling to room temperature. It was filtered and the residue washed severally with deionized water and ethanol. The residue was dried overnight in the oven at 105 °C.

2.3. Characterisation of ZnO-MgO-NiO@Stearicamide

The ZnO-MgO-NiO@Stearicamide was characterised on FTIR (Perkin Elmer), SEM (coupled with EDX detector TM3000, Hitachi), TEM (200

kV FEG, Talos F200X G2), XRD (Panalytical Empyrean (Cu radiation), measured at range 5.00–90.00° (2θ)), BET surface area which was determined by N₂ gas adsorption (Micromeritics, TriStar II 3020 version 3.02) and TG analysis (carried out on TGA Q500 V20).

2.4. Batch adsorption study

The adsorption by ZnO-MgO-NiO@Stearicamide was carried out using solutions containing 1.00 to 10.00 mg L⁻¹ CIP or AMP. The sorption was achieved in a 250 mL conical flask containing 100 mL test solution at 298 K, shaking at 150 rpm for 2 h while the ZnO-MgO-NiO@Stearicamide weight was kept at 0.1 g. To monitor the sorption process, clear samples of either CIP or AMP were collected at interval to estimate adsorption capacity of ZnO-MgO-NiO@Stearicamide. The percentage removal expressed towards CIP and AMP was determined using UV-visible spectrophotometer (UV-2550, Shimadzu Corporation) with a pre-determined calibration curve for CIP and AMP. The spectrophotometric measurements for CIP ($\lambda_{\text{max}} = 247 \text{ nm}$) and AMP ($\lambda_{\text{max}} = 232 \text{ nm}$) were taken at their maximum absorbance wavelength.

The pH effect on the sorption of CIP and AMP by ZnO-MgO-NiO@Stearicamide was studied by varying pH from 1 to 12 at an initial concentration of 10.00 mg L⁻¹, weight of 0.1 g, temperature of 298 K and a shaking rate of 150 rpm for 2 h. The weight of ZnO-MgO-NiO@Stearicamide was varied between 0.1 and 0.5 g in order to determine its effect on the sorption rate. During this process, the initial concentration was kept as 10.00 mg L⁻¹, initial pH was 7.2 for CIP and 7.60 for AMP, temperature was 298 K and the shaking was conducted at 150 rpm for 2 h. Furthermore, the effect of temperature was checked by varying the temperature from 298 – 323 K.

From the experimental data, the adsorption capacity of ZnO-MgO-NiO@Stearicamide towards CIP and AMP as well as the percentage removal of CIP and AMP were calculated as shown in Eq. 1(a-d).

$$q_t = \frac{(C_o - C_t)V}{m} \quad (1a)$$

$$q_e = \frac{(C_o - C_e)V}{m} \quad (1b)$$

$$\text{Removal (\%)} = \frac{(C_o - C_t)}{C_o} \times 100 \quad (1c)$$

$$q_t = \frac{(\% \text{removal} \times C_o \times V)}{100 \times m} \quad (1d)$$

where q_t (mg g⁻¹) and q_e (mg g⁻¹) are the adsorption capacities of ZnO-MgO-NiO@Stearicamide at time t , and equilibrium, respectively. C_o , C_t and C_e are the initial, time t and equilibrium concentration (mg L⁻¹) of CIP or AMP, respectively. The weight of ZnO-MgO-NiO@Stearicamide is represented as m and volume of test solution represented as V (L).

2.5. Desorption study

The desorption of CIP and AMP from the surface of ZnO-MgO-NiO@Stearicamide was studied via chemical regeneration method as previously described [33]. This involved the use of solvent system for the removal of CIP and AMP from the surface of ZnO-MgO-NiO@Stearicamide. Solvents used are H₂O, CH₃OH and HCl (0.5 M) which were selected based on the solubility of CIP and AMP. The sorption of CIP or AMP by ZnO-MgO-NiO@Stearicamide was repeated at initial concentration of 10.00 mg L⁻¹, temperature of 298 K, weight 0.1 g and shaken at 150 rpm for 2 h in a 250-mL conical flask and at their initial pH. The mixture was filtered using 0.22-μm Whatman membrane filter. The residue, ZnO-MgO-NiO@Stearicamide-adsorbate (CIP/AMP) obtained was air-dried for 24 h. The dried ZnO-MgO-NiO@Stearicamide-adsorbate (CIP/AMP) was poured separately into 250-mL conical flask containing 100 mL of either H₂O, C₂H₅OH, or HCl

(0.5 M) at 303 K, shaken for 2 h at 150 rpm and filtered. The amount of CIP or AMP desorbed was determined spectrophotometrically using UV-visible spectrophotometer (UV-2550, Shimadzu Corporation) and calculated using the following equation:

$$\text{Desorption}(\%) = \frac{q_d(\text{desorption})}{q_a(\text{adsorption})} \times 100 \quad (2)$$

q_d and q_a represent the amount of CIP or AMP desorbed from ZnO-MgO-NiO@Stearicamide and the amount of CIP or AMP adsorbed by ZnO-MgO-NiO@Stearicamide at equilibrium, respectively.

2.6. Quantum chemical investigation

The removal of CIP and AMP by ZnO-MgO-NiO@Stearicamide was further investigated employing Density Functional Theory (DFT) involving electronic structure programs (B3LYP/6-31G on Spartan 14.1 software). The electronic structures of CIP and AMP were modelled to understand the sorption of CIP and AMP by ZnO-MgO-NiO@Stearicamide taking into account the highest occupied molecular orbital (HOMO) and the lowest unoccupied molecular orbital (LUMO) of CIP and AMP.

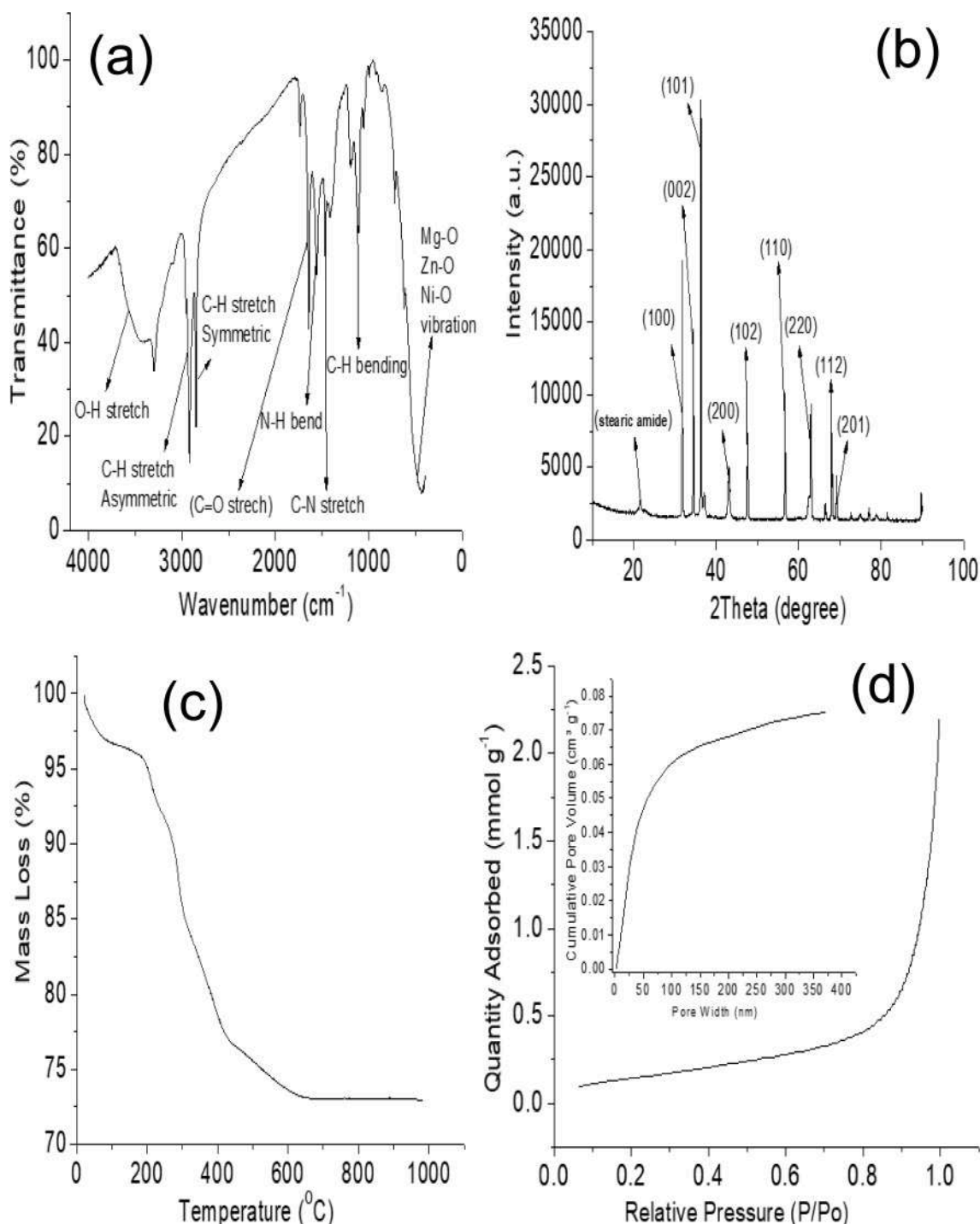


Fig. 2. Characteristics of ZnO-NiO-MgO@stearicamide, (a) FTIR, (b) XRD, (c) TGA and (d) BET.

3. Results and discussion

3.1. Synthesis and characterization of ZnO-MgO-NiO@Stearicamide

The functional groups in ZnO-MgO-NiO@Stearicamide were determined using FTIR and the result is shown in Fig. 2a. The FTIR reveals a peak at 3473 cm^{-1} which is attributed to OH stretching. Two peaks appearing at 2931 and 2892 cm^{-1} are attributed to asymmetric and

symmetric C—H stretching of alkane emanating from stearic amide, respectively. The peak at 1721 cm^{-1} is assigned to the C=O stretching of carbonyl group in amide which confirms the presence of stearic amide in the structure of ZnO-MgO-NiO@Stearicamide. The peaks at 1573 and 1462 cm^{-1} are considered to be due to the N—H in plane bending and C—N stretching of amide, respectively while the signal at 1123 cm^{-1} is attributed to the C—H bending of long chain alkane from the stearic amide which is an 18-carbon chain molecule. The peak that appears at

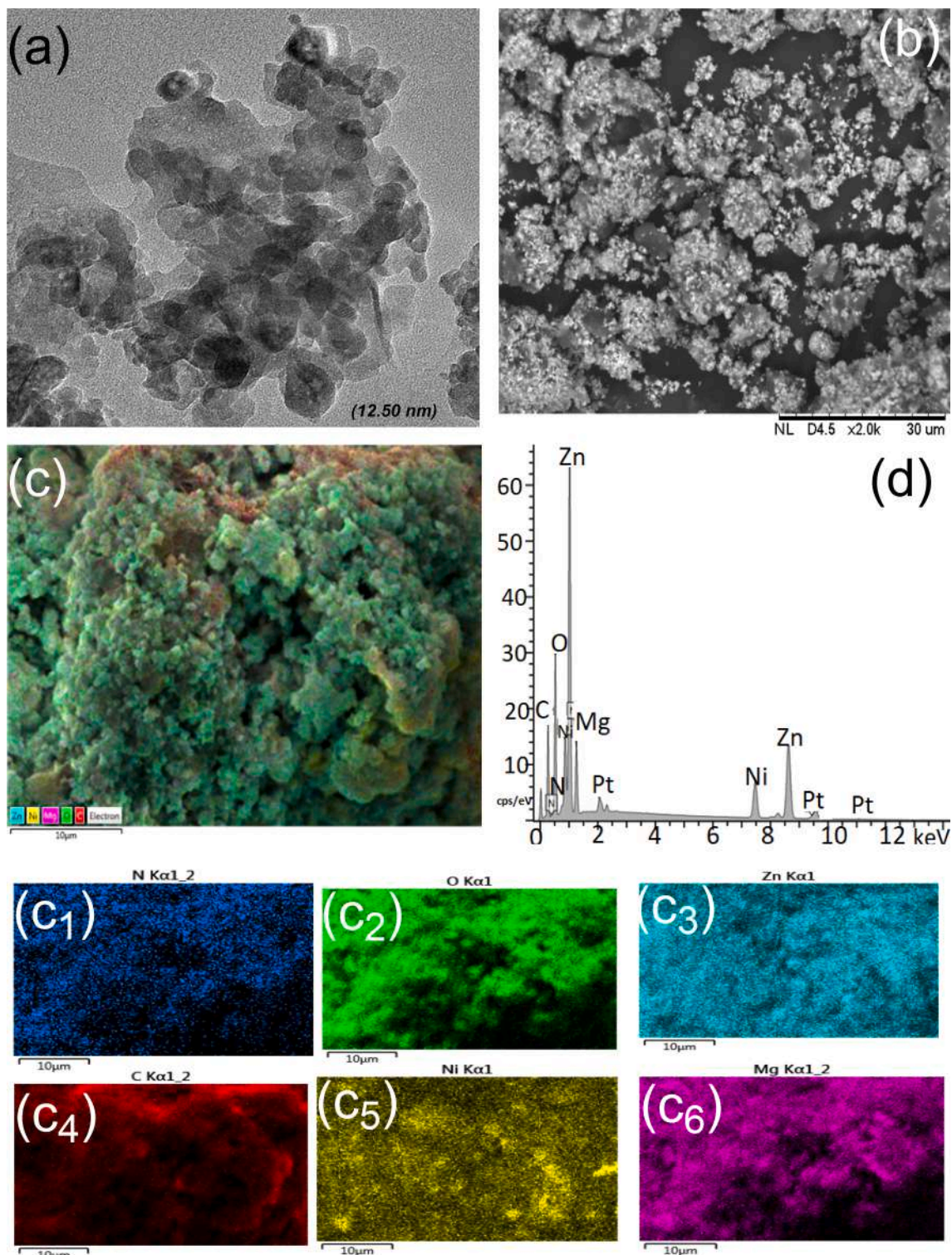


Fig. 3. (a) TEM, (b) SEM, (c) Surface mapping and (d) EDS spectra of ZnO-NiO-MgO@stearicamide.

498 cm^{-1} is attributed to the stretching modes for metal oxides which include Zn-O, Mg-O and Ni-O [21,34,35]. The X-ray diffraction pattern of ZnO-MgO-NiO@Stearicamide as shown in Fig. 2b is corresponded to the Miller index of (100), (002), (101), (200), (102), (110), (220), (112) and (201). The most intense peak is found at $2\theta = 37.06^\circ$ which corresponds to (101). The signal at $2\theta = 21.61^\circ$ confirms the presence of stearic amide as previously reported [36]. The Debye-Scherrer's formula (as expressed in Eq. (3)) considering the reflections of (101) is employed in calculating the crystallite size of ZnO-MgO-NiO@Stearicamide, D [37]:

$$D = \frac{K\lambda}{\beta \cos\theta} \quad (3)$$

From Eq. (3), K is a constant (0.89) while the X-ray wavelength (1.5406 Å) is represented as λ . The full width of diffraction line at half of the maximum intensity (FWHM) is given as β and the Bragg's angle (in radian) at peak (101) is represented as θ [38]. The crystallite size of ZnO-MgO-NiO@Stearicamide is found to be 25.93 nm.

The thermogram as shown in Fig. 2c reflects the thermal stability of ZnO-MgO-NiO@Stearicamide at different temperatures. The loss in the range 20–100 °C and 100–210 °C may be attributed to loss of adsorbed water and volatile molecules. The loss seen at 210–400 °C could be assigned to loss of stearic amide molecule [36]. The BET surface area of ZnO-MgO-NiO@Stearicamide is found to be 13.50 $\text{m}^2 \text{g}^{-1}$ from the N_2 adsorption-desorption isotherm of the material which is presented in Fig. 2d. The total pore volume (at $P/P_0 = 0.900$) and adsorption average pore diameter are reported to be 0.076 $\text{cm}^3 \text{g}^{-1}$ and 22.62 nm, respectively. The isotherm may be described as type II and typical of mesoporous adsorbents [39].

The TEM micrograph as shown in Fig. 3a reveals an average particle size of 12.50 nm with spherically shape. The SEM micrograph shows some white patches on the surface ZnO-MgO-NiO@Stearicamide which indicate the surface to be heterogeneous. Fig. 2c and d reveal the surface mapping and the EDS of ZnO-MgO-NiO@Stearicamide with respect to C, N, O, Zn, Ni and Mg element. Pt element is also detected during the analysis because it is used as coating material for the ZnO-MgO-NiO@Stearicamide to enhance the electrical conductivity and the quality of the micrographs.

3.2. Adsorption process

The molecular structures of CIP and AMP are shown in Fig. 4 while Fig. 5 compares the adsorption capacities of ZnO-MgO-NiO@Stearicamide against CIP and AMP and their percentage removal. An equilibrium time for the sorption process is established after 40 min for CIP while in the case of AMP the equilibrium sorption time is after 55 min. The findings are achieved after several trials. It is observed that the adsorption capacity expressed by ZnO-MgO-NiO@Stearicamide towards CIP and AMP increases with increasing CIP and AMP concentration from 1.00 to 10.00 mg L^{-1} whereas the percentage removal increases with a decrease in concentration of CIP and AMP. However, both adsorption capacity and percentage removal increase with increase in the experimental time from 0 to 120 min. The observed increase in adsorption capacity as concentration of CIP and AMP increases might be due to the fact that more species of CIP and AMP

are available for interaction with the surface of ZnO-MgO-NiO@Stearicamide as concentration increases. On the other hand, in the case of percentage removal, the amount of CIP and AMP species in solution reduced with reduction in concentration which means that lesser amount of CIP and AMP species were present in solution as concentration reduced. Therefore, reducing the workload on ZnO-MgO-NiO@Stearicamide and thus increase in percentage removal. The adsorption capacity towards CIP is 8.39 mg g^{-1} while that of AMP is 8.10 mg g^{-1} .

The effect of solution pH and weight of ZnO-MgO-NiO@Stearicamide on the removal of CIP and AMP is presented in Fig. 6. The adsorption capacity and percentage removal are found to increase with increasing solution pH from 1 to 7. After pH 7, the adsorption capacity as well as the percentage removal are negatively affected under alkaline environment. Previous study has shown the pKa of CIP to be 6.1 and 8.7 for the carboxylic and amine groups in its molecule (see Fig. 4), respectively [40,41]. Furthermore, other studies have also shown that when solution pH is above 8.7, proton from the carboxylic group is loss and CIP becomes anionic [42,43]. Therefore, as pH is increased from 1 to 6.1, CIP gradually becomes positively charged for interaction with the hydroxyl group on the surface of ZnO-MgO-NiO@Stearicamide. Moreover, as pH changes from 6.1 to 8.7, CIP exists as zwitterion [40,41] with ZnO-MgO-NiO@Stearicamide exhibiting the highest removal of CIP at pH 7.

Similarly, the removal of AMP is enhanced with increase in pH from 1 to 7. The pKa for AMP is 2.5 for the carboxylic group and 7.3 for the amine group. In both CIP and AMP, the interaction with the surface of ZnO-MgO-NiO@Stearicamide is facilitated by electronic interaction as the ionic state changes with change in pH with maximum removal achieved at pH 7. This mechanism of interaction is further illustrated as shown in Fig. 7. Varying the weight of ZnO-MgO-NiO@Stearicamide had effect on the removal of CIP and AMP from solution. Increasing weight from 0.1 to 0.5 g leads to an increase in the percentage removal of both CIP and AMP (Fig. 6 c and d). This observation may be due to the fact that as weight of ZnO-MgO-NiO@Stearicamide is increased, there are more active sites available for the CIP and AMP sorption. On the contrary, increasing the weight of ZnO-MgO-NiO@Stearicamide negatively affects adsorption capacity which maybe mathematically explained as shown in Eq. (1d), i.e., as weight increases, the size of the denominator in Eq. (1d) increases which had more effect on the final value of the adsorption capacity. However, ZnO-MgO-NiO@Stearicamide being efficient at low weight is advantageous because of the competitiveness of using this material.

3.3. Process kinetic models

The experimental data generated from the sorption of CIP and AMP by ZnO-MgO-NiO@Stearicamide are modelled for pseudo-first and pseudo-second-orders kinetic models as well as Elovich and intra-particle diffusion models to understand better the sorption of CIP and AMP by ZnO-MgO-NiO@Stearicamide. Pseudo-first-order is described as:

$$\log(q_e - q_t) = \log q_e - \frac{k_1}{2.303} t \quad (4)$$

while the pseudo-second-order is given as:

$$\frac{t}{q_t} = \frac{1}{k_2 q_e^2} + \frac{1}{q_e} t \quad (5)$$

From both equations, q_t (mg g^{-1}) and q_e (mg g^{-1}) are the adsorption capacity of ZnO-MgO-NiO@Stearicamide at time t and equilibrium, respectively, t is time (min) while k_1 (min^{-1}) and k_2 ($\text{g mg}^{-1} \text{min}^{-1}$) are 1st and 2nd order the rate constant, respectively. For the 1st order, $\log(q_e - q_t)$ is plotted against t while $\frac{t}{q_t}$ is plotted against t for the 2nd order model with a slope of $(\frac{1}{k_2 q_e^2})$ and intercept of $(\frac{1}{q_e})$. The r^2 values obtained

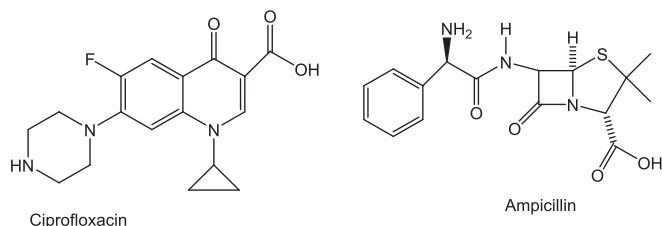


Fig. 4. Organic structures of ciprofloxacin and ampicillin.

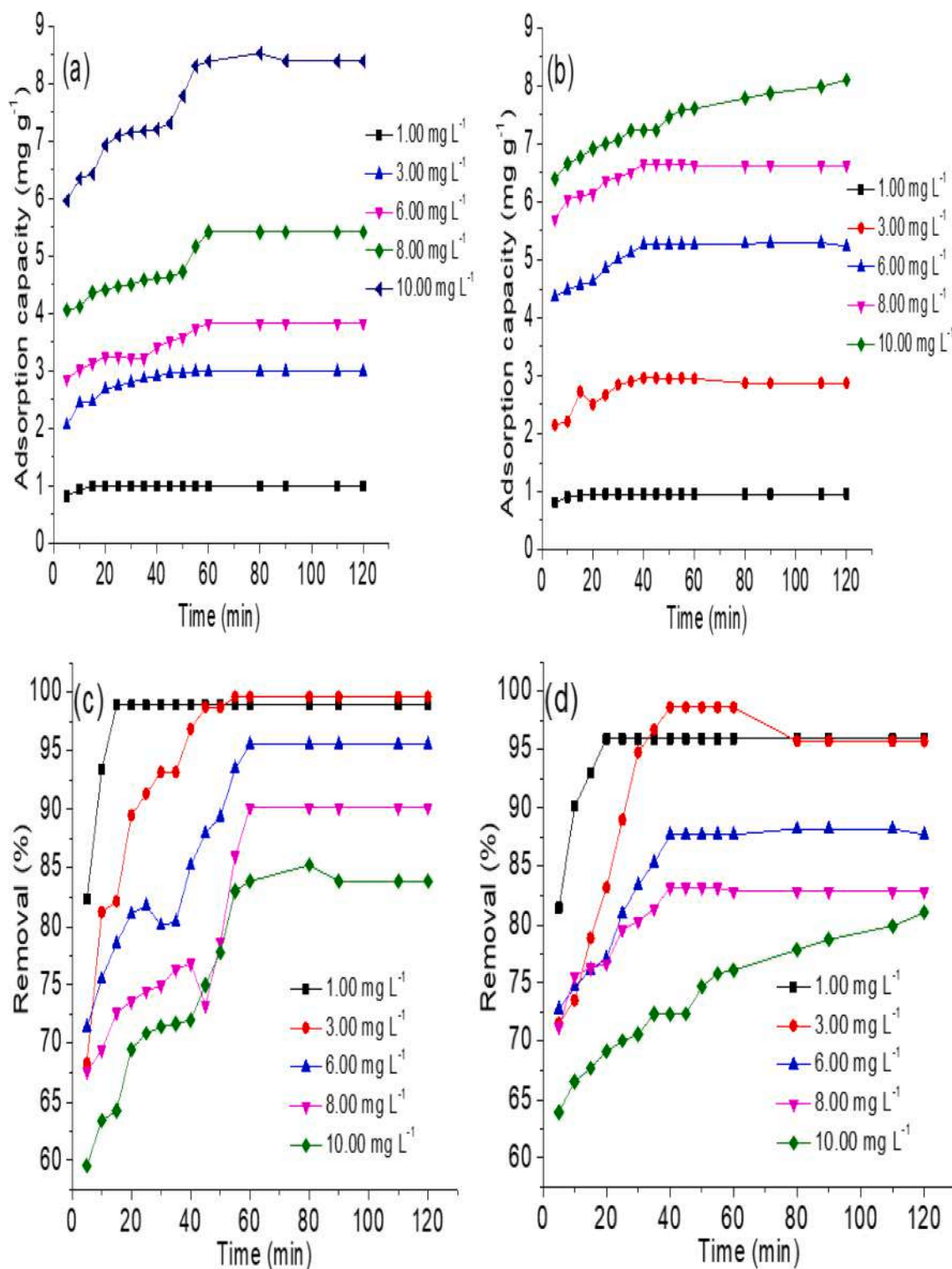


Fig. 5. Comparison of the adsorption capacity (a = CIP and b = AMP) and removal rate (c = CIP and d = AMP) of ZnO-NiO-MgO@stearicamide at different concentration.

from the plot reveal that data fitted better for the pseudo-second-order model than the pseudo-first-order model in the sorption of CIP and AMP. Furthermore, the q_e values obtained from the pseudo-second-order model for both CIP (8.83 mg g⁻¹) and AMP (8.19 mg g⁻¹) are closely related to the experimental values as shown in Table 1 along with values obtained for other parameters. The data are further subjected to an intra-particle diffusion model described as:

$$q_t = k_{id}t^{1/2} + C \quad (6)$$

where k_{id} (mg g⁻¹ min^{1/2}) and C (mg g⁻¹) represents the diffusion rate constant and layer thickness, respectively. These parameters are determined from the plot of q_t against $t^{1/2}$, and their values are presented in Table 1. The r^2 values are 0.91 for CIP and 0.99 for AMP, suggesting that the sorption that has taken place could be further described by intra-

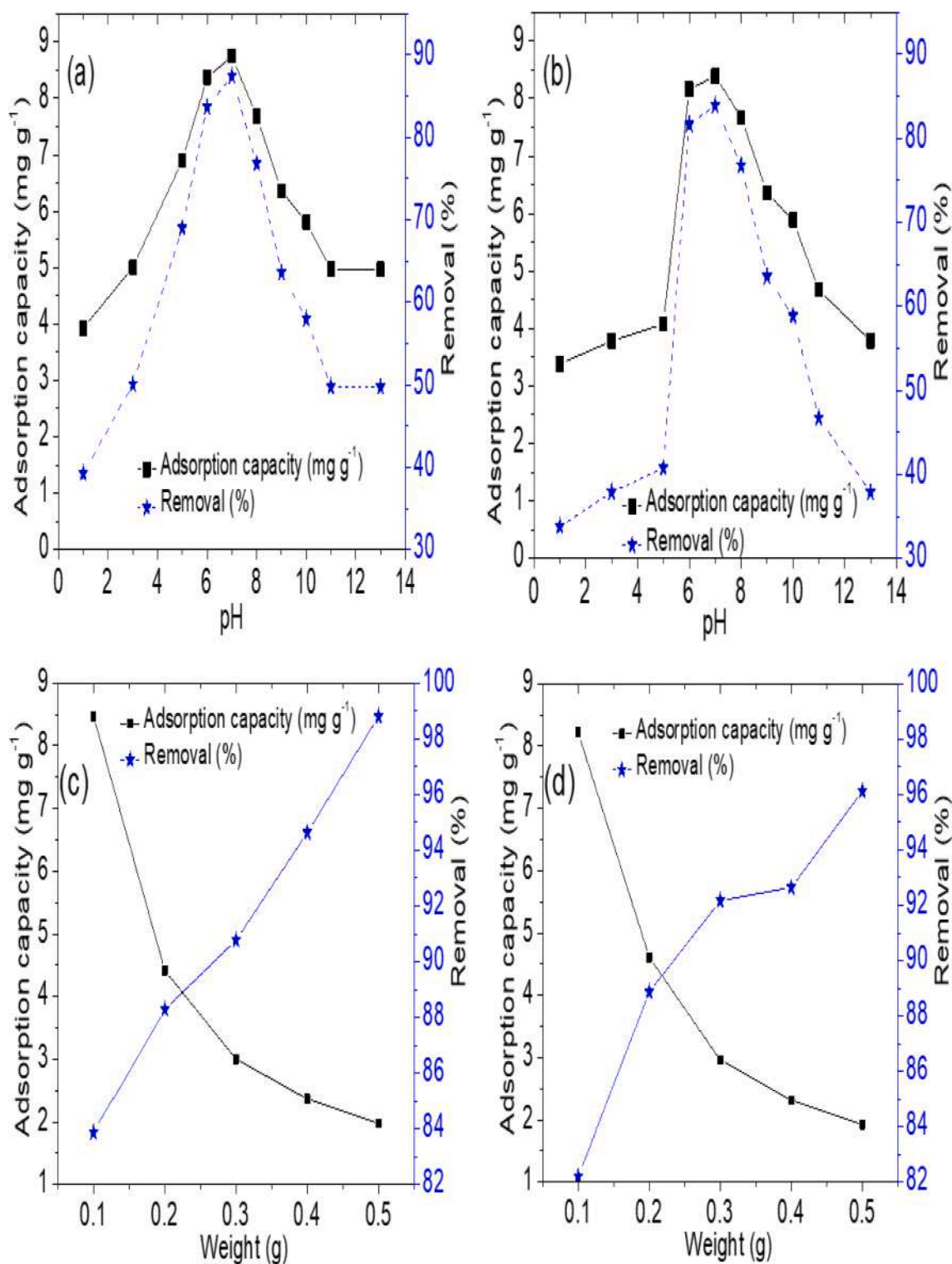


Fig. 6. Effect of solution pH (a = CIP & b = AMP) and ZnO-NiO-MgO@stearicamide weight (c = CIP & d = AMP) on the adsorption capacity and removal rate of CIP and AMP.

particle diffusion [44]. Firstly, the diffusion of the species of CIP and AMP through the solution to the mesopores and macropores of ZnO-MgO-NiO@Stearicamide and secondly, the gradual and continuous sorption of CIP and AMP until equilibrium is reached. During this second stage, the intra particle diffusion is the rate limiting step. In overall, during the two stages, species of CIP and AMP are gradually adsorbed in the micropores of ZnO-MgO-NiO@Stearicamide.

The sorption process can also be described by the Elovich model,

which in its linearised form can be expressed as:

$$q_t = \frac{1}{\beta} \ln(\alpha\beta) + \frac{1}{\beta} \ln t \quad (7)$$

the plot of q_t versus $\ln t$ is estimated for the determination of initial rate of adsorption, α (mg g⁻¹ min⁻¹) and magnitude of coverage, β (g mg⁻¹). The results obtained are presented in Table 1.

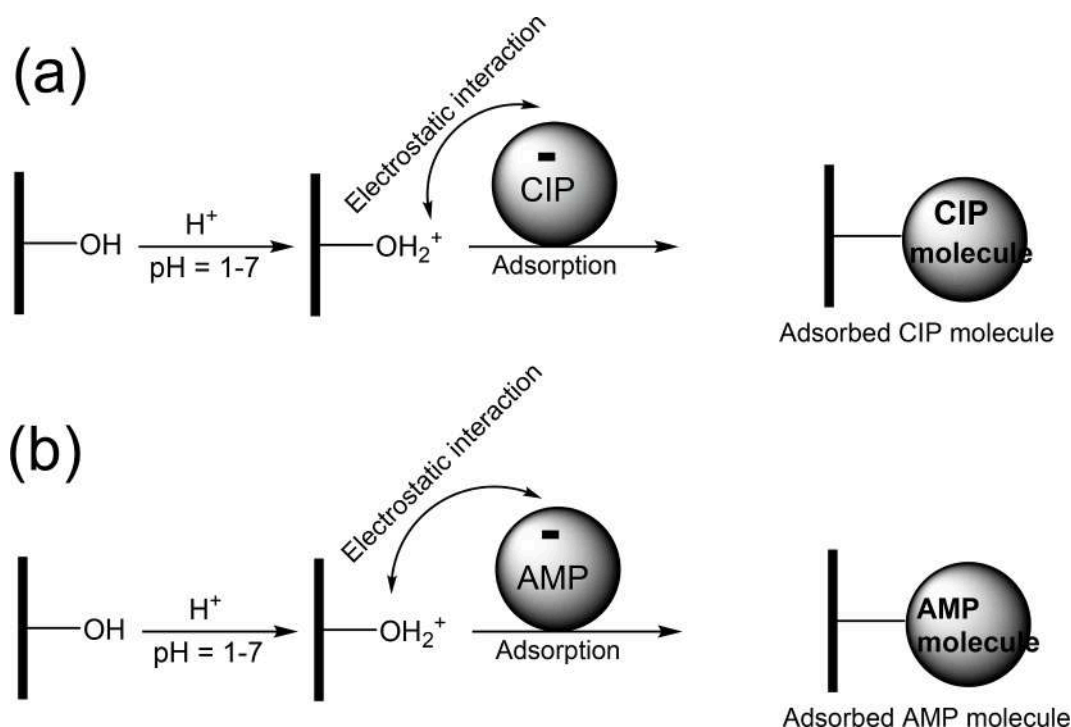


Fig. 7. Adsorption mechanism for the removal of CIP (a) and AMP (b) molecules from solution.

Table 1

Kinetic model parameters for the sorption of CIP and AMP from solution by ZnO-NiO-MgO@Stearicamide.

Model	Parameters	CIP	AMP
Pseudo-First-order	q_e (mg g^{-1})	3.91	2.09
	k_1 (min^{-1})	0.04	0.02
	r^2	0.62	0.96
Pseudo-second-order	q_e (mg g^{-1})	8.83	8.19
	k_2 ($\text{g mg}^{-1} \text{min}^{-1}$)	0.02	0.05
	r^2	0.99	0.99
	($\text{mg g}^{-1} \text{min}$)	1.63	2.99
Intra-particle diffusion	k_{id} ($\text{mg g}^{-1} \text{min}^{1/2}$) C	0.30	0.19
	(mg g^{-1})	5.44	6.03
	r^2	0.91	0.99
Elovich	β (g mg^{-1}) α	0.23	0.19
	($\text{mg g}^{-1} \text{min}^{-1}$)	2.42	1.74
	r^2	0.90	0.96
Experiment	q_e (mg g^{-1})	8.39	8.10

3.4. Isotherms study

The experimental data are further subjected to Langmuir and Freundlich isotherm models. Langmuir isotherm model is given as follows [45]:

$$\frac{C_e}{q_e} = \frac{1}{Q_o} C_e + \frac{1}{Q_o K_L} \quad (8)$$

where C_e (mg L^{-1}) is the equilibrium concentration of CIP or AMP, q_e (mg g^{-1}) is the adsorption capacity of ZnO-MgO-NiO@Stearicamide at equilibrium, while the Langmuir isotherm constant is represented as (L mg^{-1}). Q_o (mg g^{-1}) represents the maximum monolayer coverage capacity exhibited by ZnO-MgO-NiO@Stearicamide. A straight line could be obtained from C_e/q_e vs C_e plot. The values of Q_o (slope = $1/Q_o$) and K_L (intercept = $1/Q_o K_L$) are then determined from the graph and the results are presented in Table 2. The r^2 values obtained show that experimental data are well-fitted and the process could be described by the Langmuir model. The Q_o value obtained is 8.39 mg g^{-1} for CIP and 8.10 mg g^{-1} for AMP, which is closely related to the experimental values

Table 2

CIP and AMP sorption parameters for Langmuir and Freundlich models.

Isotherm	CIP	AMP
Langmuir		
Q_o (mg g^{-1})	8.39	8.10
K_L (L mg^{-1})	1.19×10^4	6.17×10^3
r^2	0.99	0.99
R_L	8.39×10^{-6}	1.62×10^{-5}
Freundlich		
K_f (L mg^{-1})	10.20	10.36
$1/n$	0.36	0.36
r^2	0.96	0.98

obtained. The values obtained for the sorption heat (K_L) for CIP ($1.19 \times 10^4 \text{ L mg}^{-1}$) and AMP ($6.17 \times 10^3 \text{ L mg}^{-1}$) are presented in Table 2. The Langmuir isotherm feature (R_L) helps in understanding process suitability which can be described as:

$$R_L = \frac{1}{1 + K_L C_o} \quad (9)$$

where C_o (mg L^{-1}) and K_L stand for the initial concentration of CIP or AMP and Langmuir constant, respectively. Previous study has shown that when the $R_L > 1$, Langmuir is unfavoured but becomes favoured when the value falls between $0 < R_L < 1$ [46].

Interestingly, the process is considered linear when $R_L = 1$ and when $R_L = 0$, the process is considered irreversible. The R_L values in the sorption of CIP (8.39×10^{-6}) and AMP (1.62×10^{-5}) falls in the range $0 < R_L < 1$, suggesting that the sorption of CIP and AMP by ZnO-MgO-NiO@Stearicamide can be described by the Langmuir isotherm model, indicating that CIP and AMP must have form a monolayer on ZnO-MgO-NiO@Stearicamide. The Freundlich isotherm model can be described as follows:

$$q_e = K_F C_e^{1/n} \quad (10)$$

On plotting $\ln q_e$ against $\ln C_e$ a straight line is obtained with an r^2 value of 0.959 for CIP and 0.984 for AMP. These values suggest

compliance with Freundlich isotherm model which reveals that the surface of ZnO-MgO-NiO@Stearicamide may be heterogeneous towards the removal of CIP and AMP from solution [47]. The value of $1/n$ is important in understanding the strength of the sorption process. It may be described that when the value of $1/n = 1$, then the sorption process can be described to be independent of the concentration of CIP and AMP in solution. On the other hand, when value of $1/n$ is <1 , the sorption process may be described as being normal but if $1/n$ is >1 the sorption process may be described as cooperative adsorption process [48]. As shown in Table 2, the current study for the sorption of CIP and AMP by ZnO-MgO-NiO@Stearicamide falls in the range of $1/n < 1$, suggesting the mechanism as a normal sorption process. Obviously, the sorption of CIP and AMP by ZnO-MgO-NiO@Stearicamide can be described by both Langmuir and Freundlich isotherms.

3.5. Thermodynamics of the adsorption of CIP and AMP

The effect of temperature on the performance of ZnO-MgO-NiO@Stearicamide for the removal of CIP and AMP from aqueous solution was evaluated at different temperature and the results are presented in Table 3. It is observed that the percentage removal is increased with increasing operating temperature. It is increased from 83.87 % at 303 K to 99.22 % at 323 K in the case of CIP and from 81.04 % at 303 K to 90.03 % at 323 K in the case of AMP. This may be due to the fact that as temperature increases, the average kinetic energy of the species of CIP and AMP in solution increases accordingly which facilitates their migration to the surface of ZnO-MgO-NiO@Stearicamide and promotes interaction. The ΔG° values obtained for CIP and AMP are negative which suggest that the sorption processes are spontaneous. The ΔG° values ranged from 0 to -20 kJ mol^{-1} for both CIP and AMP, indicating the process is taking place by physisorption as previously reported [49]. The sorption process equilibrium constant (b_o), entropy change (ΔS°) and enthalpy change (ΔH°) are estimated as follows (Eqs. 13–15).

$$b_o = \frac{q_e}{C_e} \quad (11)$$

$$\Delta G^\circ = -RT \ln b_o \quad (12)$$

$$\Delta G^\circ = \Delta H^\circ - T\Delta S^\circ \quad (13)$$

where R is the gas constant ($8.314 \text{ J mol}^{-1} \text{ K}^{-1}$), C_e is equilibrium amount (mg L^{-1}), q_e is adsorption equilibrium capacity (mg g^{-1}) and T is temperature (K). Values of ΔH° and ΔS° are calculated from the plot of $\ln b_o$ vs $1/T$. As revealed in Table 4, the ΔH° value obtained for the removal of CIP ($-105.95 \text{ kJ mol}^{-1}$) and AMP ($-28.16 \text{ kJ mol}^{-1}$) are negative which suggests the process to be exothermic. The ΔS° values for both CIP ($-0.319 \text{ kJ mol}^{-1} \text{ K}^{-1}$) and AMP ($-0.076 \text{ kJ mol}^{-1} \text{ K}^{-1}$) are also negative, indicating a less disordered configuration of CIP and AMP on the surface of ZnO-MgO-NiO@Stearicamide.

Table 5 compares the capacity of ZnO-MgO-NiO@Stearicamide to remove CIP and AMP from solution with other materials that were previously reported in literature. ZnO-MgO-NiO@Stearicamide

Table 3

ΔG° and percentage removal obtained at various temperatures for the sorption of CIP and AMP on ZnO-NiO-MgO@Stearicamide.

CIP					
T (K)	303	308	313	318	323
Removal (%)	83.87	84.42	88.56	88.67	99.22
ΔG° (kJ mol^{-1})	-12.207	-5.269	-5.326	-4.468	-4.427
AMP					
T (K)	303	308	313	318	323
Removal (%)	81.04	81.62	83.65	86.84	90.03
ΔG° (kJ mol^{-1})	-5.543	-4.832	-4.248	-3.941	-3.901

Table 4

Thermodynamic parameters obtained from plot of $\ln b_o$ vs $1/T$ for sorption of CIP and AMP on ZnO-NiO-MgO@Stearicamide.

Parameters	CIP	AMP
ΔH° (kJ mol^{-1})	-105.945	-28.164
ΔS° ($\text{kJ mol}^{-1} \text{ K}^{-1}$)	-0.319	-0.076

compared favourably with previously reported materials with percentage removal that is above 80 %. Balarak et al [41] reported an adsorption capacity (9.98 mg g^{-1}) which is slightly higher than that of ZnO-MgO-NiO@Stearicamide (8.39 mg g^{-1}) for the removal of CIP; however, the performance of ZnO-MgO-NiO@Stearicamide is higher than MgO [50] and coal fly ash [44]. Adsorption capacities of 8.86 and 8.30 mg g^{-1} reported respectively for groundnut shell powder and ZnO particles [51] for CIP are close to the values obtained for ZnO-MgO-NiO@Stearicamide in this study for the removal of CIP from aqueous solution. The use of activated carbon shows an AMP adsorption capacity of 3.10 mg g^{-1} and removal rate of 73 % in previous study [52]. However, the use of ZnO-MgO-NiO@Stearicamide in this current study is better than that of activated carbon for the AMP removal. ZnO-MgO-NiO@Stearicamide exhibits better adsorption capacity towards AMP than the use of anionic surfactant reported by Boukhelkhal et al [53]. Although FGOA [54] and PZI [55] exhibit better results than ZnO-MgO-NiO@Stearicamide but the cheap synthesis route and regeneration stability of ZnO-MgO-NiO@Stearicamide makes it advantageous over these materials. Most previous study reported electrostatic interaction as the mechanism for the sorption process just like in the present study that revealed the sorption of CIP and AMP to have taken place via electrostatic interaction.

3.6. Desorption and regeneration capacities of ZnO-MgO-NiO@Stearicamide

The ability to reuse any material as adsorbent in water purification is very important in determining their economic viability. ZnO-NiO-MgO@Stearicamide is further studied for its desorption and regeneration capacities for the removal of CIP and AMP from solution. The results obtained are presented in Fig. 8. Chemical regeneration process using solvents is carried out to desorb CIP and AMP from the surface of ZnO-NiO-MgO@Stearicamide. Solvents (H_2O , CH_3OH and 0.5 M HCl) used are selected based on solubility of CIP and AMP. It is obvious that both CIP and AMP are better desorbed from the surface of ZnO-NiO-MgO@Stearicamide by HCl as seen in Fig. 8a. HCl is a cheap mineral acid that is readily available which makes the desorption process cost effective. The regeneration of ZnO-NiO-MgO@Stearicamide for continuous use as adsorbent for the removal of CIP and AMP shows a regeneration capacity which is above 80 % even at the 11th regeneration cycle. The regeneration exhibited by ZnO-NiO-MgO@Stearicamide towards CIP and AMP shows a consistent pattern which is fairly stable over the test period. This shows the possibility of ZnO-NiO-MgO@Stearicamide being a potential adsorbent with economic viability for the removal of CIP and AMP from solution.

3.7. Quantum chemical computations

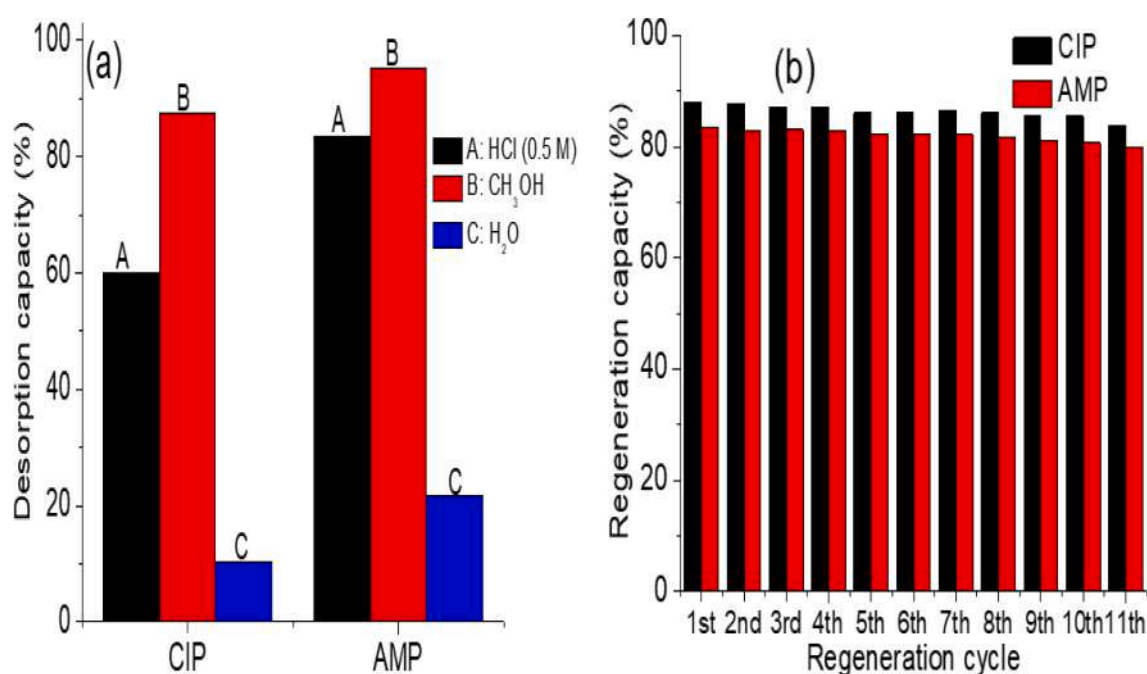
The interaction leading to the sorption of CIP and AMP by ZnO-NiO-MgO@Stearicamide is further investigated via quantum chemical computation to describe the process. The optimized geometry, HOMO, LUMO, electrical and Mulliken charge of CIP and AMP are presented in Fig. 9. The presence of heteroatoms such as oxygen, nitrogen, and sulphur are revealed in their optimized geometry. These heteroatoms can serve as sources of non-bonding electrons that may promote electrostatic interaction between the surface of ZnO-NiO-MgO@Stearicamide and the species in solution. Furthermore, the electrical and Mulliken charges suggests that the electron pairs may be

Table 5

Comparison of the CIP and AMP adsorption of ZnO-NiO-MgO@Stearicamide with other biosorbents in the literature.

Material	Adsorbate	q_e (mg g^{-1})	Adsorption isotherm	$\Delta G_{\text{ads}}^{\circ}$ (kJ/mol)	$\Delta H_{\text{ads}}^{\circ}$ (kJ/mol)	% removal	Mechanism	Reference
NiO nanoparticles	CIP	9.98	Langmuir	-4.354	6.928	99.20	-	[41]
Tamarind shells	CIP	11.04	Langmuir & Freundlich	-	-	92.00	-	[58]
Coal fly ash	CIP	1.55	Langmuir	- 5.396	28.55	-	-	[44]
MgO	CIP	3.46	Langmuir	-	-	85.00	Electrostatic interaction	[50]
Groundnut shell powder	CIP	8.86	Langmuir, Freundlich & Temkin	-	-	79.60	-	[51]
ZnO particles	CIP	8.30	-	-	-	85.40	-	-
Activated carbon	AMP	3.10	Langmuir	- 6.700	14.500	73.00	-	[52]
FGOA	AMP	294.00	Langmuir	-2.300	0.400	94.00	Electrostatic interaction	[54]
PZI	AMP	100.00	Langmuir	- 29.302	84.436	99.12	Electrostatic interaction	[55]
Anionic surfactant	AMP	2.303	Langmuir	- 2.370	5.470	59.76	Electrostatic interaction	[53]
MXenes	AMP	-	-	-	-	44.00	-	[59]
ZnO-NiO-MgO@stearic amide	CIP	8.39	Langmuir & Freundlich	-12.207	-105.945	83.87	Electrostatic interaction	This study
	AMP	8.10	-	-5.543	-28.164	81.10	-	-

- = Not reported.

PZI = Polydopamine/zirconium(IV) iodate, FGOA = Nanometer-size Fe_3O_4 /graphene oxide/aminopropyltrimethoxysilane.**Fig. 8.** Performance of ZnO-NiO-MgO@stearicamide with respect to (a) desorption and (b) regeneration.

involved in electronic interaction. The energy gap (ΔE) and hardness (η) are determined using Eq. (14) and Eq. (15), respectively.

$$\Delta E = E_{\text{LUMO}} - E_{\text{HOMO}} \quad (14)$$

$$\eta = \frac{E_{\text{LUMO}} - E_{\text{HOMO}}}{2} \quad (15)$$

The values obtained are then presented in Table 6. The dipole moment of CIP (10.62 debye) is higher than that of AMP (3.47 debye) which shows that both CIP and AMP are unsymmetrical and further suggest higher charge on CIP than AMP. The results are correlated to the higher adsorption capacity and percentage removal expressed by ZnO-NiO-MgO@Stearicamide towards CIP. The solvation energy of CIP and AMP is -60.43 and -54.51 kJ mol^{-1} , respectively. These low negative values obtained suggest good homogeneity of CIP and AMP in solution and their interaction with macromolecules [56,57]. Fig. 10 shows the electronic interaction within the orbitals of CIP and AMP for possible sorption on ZnO-NiO-MgO@Stearicamide which is further corroborated as described in Fig. 6. The indication of an electronic interaction supports the fact that ZnO-NiO-MgO@Stearicamide can be described as a

novel material that can be used for the treatment of an aqueous solution contaminated with CIP and AMP.

4. Conclusions

The study investigated the synthesis of ZnO-NiO-MgO@Stearicamide via simple reaction process and its role in the removal of CIP and AMP from solution. ZnO-NiO-MgO@stearicamide was characterized using FTIR, XRD, SEM, TEM, BET and EDS surface mapping while the removal of CIP and AMP from solution was evaluated by varying different parameters including feed concentration, solution pH and temperature as well as amount of particles used in solution. The BET surface area of ZnO-NiO-MgO@stearicamide was found at $13.50 \text{ m}^2 \text{ g}^{-1}$ while the TEM image showed an average particle size of 12.50 nm. The adsorption study revealed the capacity of ZnO-NiO-MgO@stearicamide towards CIP and AMP to be 8.39 and 8.10 mg g^{-1} , respectively. The sorption can be described by the Langmuir isotherm that is considered to be spontaneous. Further investigation showed that the ZnO-NiO-MgO@Stearicamide showed a regeneration capacity that was $> 80\%$ even after 11th regeneration cycle, suggesting the developed materials

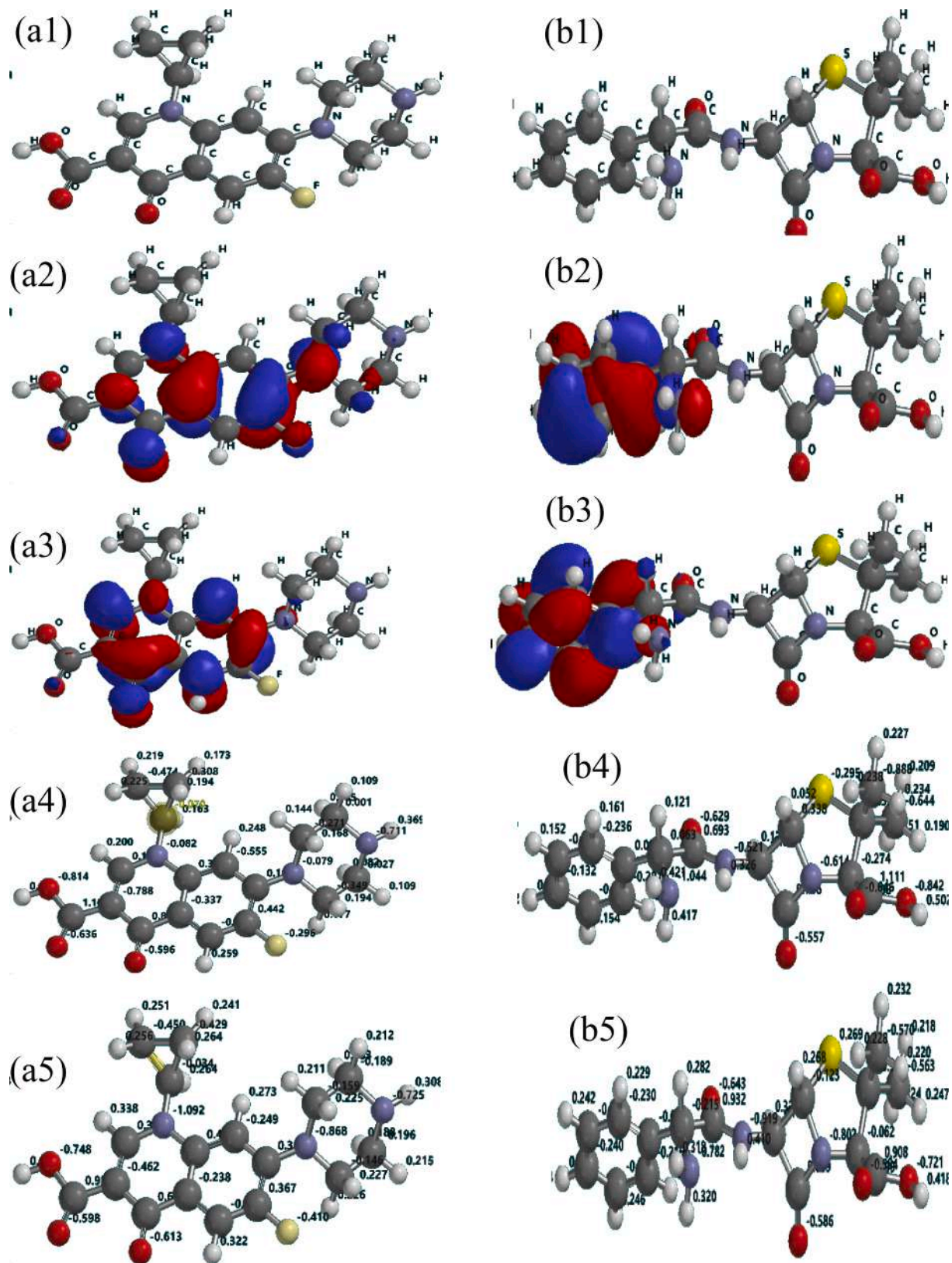


Fig. 9. Electronic properties of CIP and AMP: Optimized geometry of CIP (a1) and AMP (b1), Highest occupied molecular orbital of CIP (a2) and AMP (b2), Lowest unoccupied molecular orbital of CIP (a3) and AMP (b3), Electrical charge of CIP (a4) and AMP (b4), and Mulliken charge of CIP (a5) and AMP (b5).

Table 6

Molecular properties of CIP and AMP calculated using DFT at B3LYP/6-31G basis set level.

Quantum Chemical Property	CIP	AMP
Molecular surface area (\AA^2)	329.77	354.68
Energy (au)	-1135.24	-1469.44
E_{HOMO} (eV)	-8.35	-9.18
E_{LUMO} (eV)	2.46	3.77
$E_{\text{LUMO-HOMO}}$ (eV)	10.81	12.95
Volume (\AA^3)	316.00	329.03
Solvation energy (kJ mol^{-1})	-60.43	-54.51
Dipole moment (debye)	10.62	3.47
Group	C1	C1
Polarizability	64.47	65.03
η (eV)	5.41	6.48

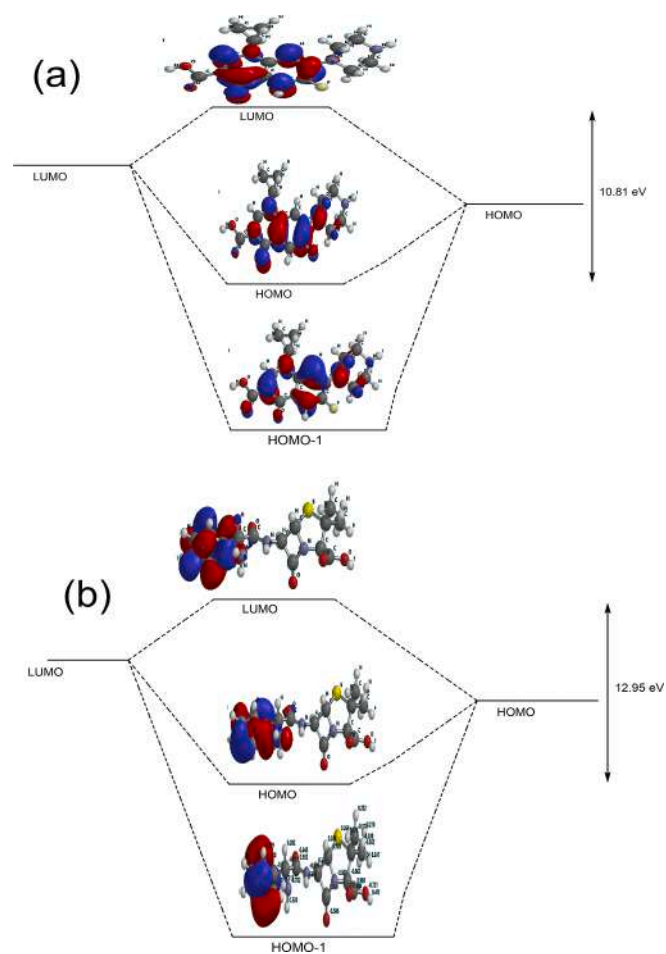


Fig. 10. Molecular orbitals of CIP (a) and AMP (b).

may be economically viable for the CIP and AMP removal. The high removal rate coupled with considerable good regeneration capacity present the ZnO-NiO-MgO@stearicamide as a potentially efficient material for the removal of CIP and AMP from contaminated water source.

CRediT authorship contribution statement

Olamide A. Olalekan: Methodology. **Abisola J. Campbell:** Methodology. **Adewale Adewuyi:** Conceptualization, Visualization, Supervision, Methodology, Writing – original draft, Investigation. **Woei Jye Lau:** Writing – review & editing. **Olalere G. Adeyemi:** Conceptualization, Visualization, Supervision, Writing – review & editing.

Declaration of Competing Interest

The authors declare that they have no known competing financial interests or personal relationships that could have appeared to influence the work reported in this paper.

Acknowledgement

Authors are grateful to the Department of Chemical Sciences, Redeemer's University, Nigeria for provision of research space and chemicals. The support received from School of Chemical and Energy Engineering, Universiti Teknologi Malaysia and Department of Chemistry, University of Cambridge, UK are highly appreciated.

References

- [1] S.I. Polianciuc, A.E. Gurzău, B. Kiss, M.G. Ștefan, F. Loghin, Antibiotics in the environment: causes and consequences, *Med. Pharm. Rep.* 93 (2020) 231.
- [2] A. Faleye, A. Adegoke, K. Ramluckan, F. Bux, T. Stenström, Antibiotic residue in the aquatic environment: status in Africa, *Open, Chemistry* 16 (2018) 890–903.
- [3] X. Guo, L.v. Xiaojun, A. Zhang, Z. Yan, S. Chen, N.a. Wang, Antibiotic contamination in a typical water-rich city in southeast China: a concern for drinking water resource safety, *J. Environ. Sci. Health, Part B* 55 (3) (2020) 193–209.
- [4] H.Q. Anh, T.P.Q. Le, N. Da Le, X.X. Lu, T.T. Duong, J. Garnier, E. Rochelle-Newall, S. Zhang, N.-H. Oh, C. Oeurng, Antibiotics in surface water of East and Southeast Asian countries: A focused review on contamination status, pollution sources, potential risks, and future perspectives, *Sci. Total Environ.* 764 (2021), 142865.
- [5] C. Liu, L. Tan, L. Zhang, W. Tian, L. Ma, A review of the distribution of antibiotics in water in different regions of china and current antibiotic degradation pathways, *Front. Environ. Sci.* 9 (2021).
- [6] C.F. Nnadozie, O.N. Odume, Freshwater environments as reservoirs of antibiotic resistant bacteria and their role in the dissemination of antibiotic resistance genes, *Environ. Pollut.* 254 (2019), 113067.
- [7] L. Serwecińska, Antimicrobials and antibiotic-resistant bacteria: a risk to the environment and to public health, *Water* 12 (2020) 3313.
- [8] J. Ma, M. Yang, F. Yu, J. Zheng, Water-enhanced removal of ciprofloxacin from water by porous graphene hydrogel, *Sci. Rep.* 5 (2015) 1–10.
- [9] M. Malakootian, M. Ahmadian, Ciprofloxacin removal by electro-activated persulfate in aqueous solution using iron electrodes, *Applied Water, Science* 9 (2019) 1–10.
- [10] M. Hassan, G. Zhu, Y.-Z. Lu, A.H. AL-Falahi, L. Yuan, S. Huang, Z. Wan, Removal of antibiotics from wastewater and its problematic effects on microbial communities by bioelectrochemical technology: current knowledge and future perspectives, *Environ. Eng. Res.* 26 (2021) 16–30.
- [11] M.S. de Ilurdoz, J.J. Sadhwani, J.V. Reboso, Antibiotic removal processes from water & wastewater for the protection of the aquatic environment—a review, *J. Water Process Eng.* 45 (2022), 102474.
- [12] X. Ma, Z. Wang, Removal of Ciprofloxacin from Wastewater by Ultrasound/Electric Field/Sodium Persulfate (US/E/PS), *Processes* 10 (2022) 124.
- [13] C. Bhagat, M. Kumar, V.K. Tyagi, P.K. Mohapatra, Proclivities for prevalence and treatment of antibiotics in the ambient water: a review, *npj Clean, Water* 3 (2020) 1–18.
- [14] Y. Fei, Y.H. Hu, Design, synthesis, and performance of adsorbents for heavy metal removal from wastewater: a review, *J. Mater. Chem. A* (2022).
- [15] U. Pal, A. Sandoval, S.I.U. Madrid, G. Corro, V. Sharma, P. Mohanty, Mixed titanium, silicon, and aluminum oxide nanostructures as novel adsorbent for removal of rhodamine 6G and methylene blue as cationic dyes from aqueous solution, *Chemosphere* 163 (2016) 142–152.
- [16] A.K. Arora, Metal/mixed metal oxides and their applications as sensors: a review, *Asian J. Res. Chem.* 11 (2018) 497–504.
- [17] W. Zhong, Design, Synthesis and Characterization of Metal Oxide Adsorbents and Catalysts for Environmental Applications, (2017).
- [18] A. Aslani, M.R. Arefi, A. Babapoor, A. Amiri, K. Beyki-Shuraki, Solvothermal synthesis, characterization and optical properties of ZnO, ZnO–MgO and ZnO–NiO, mixed oxide nanoparticles, *Appl. Surf. Sci.* 257 (2011) 4885–4889.
- [19] F. Song, L. Bai, A. Moysiadou, S. Lee, C. Hu, L. Liardet, X. Hu, Transition metal oxides as electrocatalysts for the oxygen evolution reaction in alkaline solutions: an application-inspired renaissance, *J. Am. Chem. Soc.* 140 (2018) 7748–7759.
- [20] M.S. Chavali, M.P. Nikolova, Metal oxide nanoparticles and their applications in nanotechnology, *SN applied sciences* 1 (2019) 1–30.
- [21] L.M. Anaya-Esparza, E. Montalvo-González, N. González-Silva, M.D. Méndez-Robles, R. Romero-Toledo, E.M. Yahia, A. Pérez-Larios, Synthesis and characterization of TiO₂-ZnO-MgO mixed oxide and their antibacterial activity, *Materials* 12 (2019) 698.
- [22] S. Mandal, S. Natarajan, Adsorption and catalytic degradation of organic dyes in water using ZnO/ZnxFe_{3-x}O₄ mixed oxides, *J. Environ. Chem. Eng.* 3 (2015) 1185–1193.
- [23] V. Štengl, S. Bakardjieva, M. Maříková, P. Bezdicka, J. Šubrt, Magnesium oxide nanoparticles prepared by ultrasound enhanced hydrolysis of Mg-alkoxides, *Mater. Lett.* 57 (2003) 3998–4003.

- [24] M.N. Zafar, Q. Dar, F. Nawaz, M.N. Zafar, M. Iqbal, M.F. Nazar, Effective adsorptive removal of azo dyes over spherical ZnO nanoparticles, *J. Mater. Res. Technol.* 8 (2019) 713–725.
- [25] F. Zhang, X. Chen, F. Wu, Y. Ji, High adsorption capability and selectivity of ZnO nanoparticles for dye removal, *Colloids Surf., A* 509 (2016) 474–483.
- [26] J. Hu, K. Zhu, L. Chen, H. Yang, Z. Li, A. Suchopar, R. Richards, Preparation and surface activity of single-crystalline NiO (111) nanosheets with hexagonal holes: A semiconductor nanospanner, *Adv. Mater.* 20 (2008) 267–271.
- [27] F. Motahari, M.R. Mozdianfar, M. Salavati-Niasari, Synthesis and adsorption studies of NiO nanoparticles in the presence of H2acacen ligand, for removing Rhodamine B in wastewater treatment, *Process Saf. Environ. Prot.* 93 (2015) 282–292.
- [28] N. Roya, R. Gholam, M. Mohammad, M. Hamed, Decolourization of synthetic wastewater by nickel oxide nanoparticles, *Int. J. Environ. Health Eng* 1 (2013) 1–25.
- [29] M.A. Subhan, P. Chandra Saha, N. Uddin, P. Sarker, Synthesis, structure, spectroscopy and photocatalytic studies of nano multi-metal oxide MgO• Al2O3• ZnO and MgO• Al2O3• ZnO-curcumin composite, *International, J. Nanosci. Nanotechnol.* 13 (2017) 69–82.
- [30] S. Patial, P. Raizada, V. Hasija, P. Singh, V.K. Thakur, V.-H. Nguyen, Recent advances in photocatalytic multivariate metal organic frameworks-based nanostructures toward renewable energy and the removal of environmental pollutants, *Mater. Today Energy* 19 (2021), 100589.
- [31] S. Homaeigozar, The nanosized dye adsorbents for water treatment, *Nanomaterials* 10 (2020) 295.
- [32] S.H. Paiman, M.A. Rahman, T. Uchikoshi, N. Abdullah, M.H.D. Othman, J. Jaafar, K.H. Abas, A.F. Ismail, Functionalization effect of Fe-type MOF for methylene blue adsorption, *J. Saudi Chem. Soc.* 24 (11) (2020) 896–905.
- [33] A. Adewuyi, C.A. Gervasi, M.V. Mirifico, Synthesis of strontium ferrite and its role in the removal of methyl orange, phenolphthalein and bromothymol blue from laboratory wastewater, *Surf. Interfaces* 27 (2021) 101567.
- [34] R. Viswanatha, T. Venkatesh, C. Vidyasagar, Y.A. Nayaka, Y. Arch, Preparation and characterization of ZnO and Mg-ZnO nanoparticle, *Archiv. Appl. Sci. Res.* 4 (2012) 480–486.
- [35] W.C.d. Abreu, A.F. Moraes, R.Y.N. Reis, B.F. Pinto, C.V.R.d. Moura, S. Nicolodi, E. M.d. Moura, Magnetic materials enriched with strontium: a study of the use as catalysts in the transesterification reaction of babassu oil, *Mater. Res.* 22 (suppl 1) (2019).
- [36] Y. Chen, X. Zhang, B. Wang, M. Lv, Y. Zhu, J. Gao, Fabrication and characterization of novel shape-stabilized stearic acid composite phase change materials with tannic-acid-templated mesoporous silica nanoparticles for thermal energy storage, *RSC Adv.* 7 (2017) 15625–15631.
- [37] C. Hammond, *The Basics Of Crystallography And Diffraction*, International Union of Crystal, 2015.
- [38] M. Ghaedi, E. Nazari, R. Sahaie, M. Purkait, Kinetic and isotherm study of Bromothymol Blue and Methylene blue removal using Au-NP loaded on activated carbon, *Desalination, Water Treatment* 52 (2014) 5504–5512.
- [39] K.K. Senapati, S. Roy, C. Borgohain, P. Phukan, Palladium nanoparticle supported on cobalt ferrite: An efficient magnetically separable catalyst for ligand free Suzuki coupling, *J. Mol. Catal. A: Chem.* 352 (2012) 128–134.
- [40] S.T. Danaloğlu, Ş.S. Bayazit, Ö.K. Kuyumcu, M.A. Salam, Efficient removal of antibiotics by a novel magnetic adsorbent: Magnetic activated carbon/chitosan (MACC) nanocomposite, *J. Mol. Liq.* 240 (2017) 589–596.
- [41] D. Balarak, A.H. Mahvi, M.J. Shim, S.-M. Lee, Adsorption of ciprofloxacin from aqueous solution onto synthesized NiO: isotherm, kinetic and thermodynamic studies, *Desalin, Water Treat* 212 (2021) 390–400.
- [42] E.-S.-I. El-Shafey, H. Al-Lawati, A.S. Al-Sumri, Ciprofloxacin adsorption from aqueous solution onto chemically prepared carbon from date palm leaflets, *J. Environ. Sci.* 24 (2012) 1579–1586.
- [43] C.d.O. Carvalho, D.L. Costa Rodrigues, E.C. Lima, C.S. Umperies, D.F. Caicedo Chaguezac, F.M. Machado, Kinetic, equilibrium, and thermodynamic studies on the adsorption of ciprofloxacin by activated carbon produced from Jeriva (*Syagrus romanzoffiana*), *Environ. Sci. Pollut. Res.* 26 (2019) 4690–4702.
- [44] C.-L. Zhang, G.-L. Qiao, F. Zhao, Y. Wang, Thermodynamic and kinetic parameters of ciprofloxacin adsorption onto modified coal fly ash from aqueous solution, *J. Mol. Liq.* 163 (2011) 53–56.
- [45] A. Terdputtakun, O.-A. Arqueropanyo, P. Sooksamiti, S. Janhom, W. Naksata, Adsorption isotherm models and error analysis for single and binary adsorption of Cd (II) and Zn (II) using leonardite as adsorbent, *Environ. Earth Sci.* 76 (2017) 777.
- [46] A. Adewuyi, R.A. Oderinde, Chemically modified vermiculite clay: a means to remove emerging contaminant from polluted water system in developing nation, *Polym. Bull.* 76 (2019) 4967–4989.
- [47] S. Goldberg, Equations and models describing adsorption processes in soils, *Chem. Proc. Soils* 8 (2005) 489–517.
- [48] A. Adewuyi, A.I. Ogagbalo, W.J. Lau, R.A. Oderinde, Synthesis of spinel ferrite and its role in the removal of free fatty acids from deteriorated vegetable oil, *Chin. J. Chem. Eng.* (2020).
- [49] P. Húmpola, H. Odetti, A.E. Fertitta, J.L. Vicente, Thermodynamic analysis of adsorption models of phenol in liquid phase on different activated carbons, *J. Chil. Chem. Soc.* 58 (2013) 1541–1544.
- [50] N. Khoshnamvand, S. Ahmadi, F.K. Mostafapour, Kinetic and isotherm studies on ciprofloxacin an adsorption using magnesium oxide nanoparticles, *J Appl Pharm Sci* 7 (2017) 079–083.
- [51] N. Dhiman, N. Sharma, Batch adsorption studies on the removal of ciprofloxacin hydrochloride from aqueous solution using ZnO nanoparticles and groundnut (*Arachis hypogaea*) shell powder: a comparison, *Indian Chem. Eng.* 61 (1) (2019) 67–76.
- [52] P. Del Vecchio, N.K. Haro, F.S. Souza, N.R. Marcílio, L.A. Féris, Ampicillin removal by adsorption onto activated carbon: kinetics, equilibrium and thermodynamics, *Water Sci. Technol.* 79 (2019) 2013–2021.
- [53] A. Boukhelkhal, O. Benkortbi, M. Hamadache, Use of an anionic surfactant for the sorption of a binary mixture of antibiotics from aqueous solutions, *Environ. Technol.* 40 (2019) 3328–3336.
- [54] H.T. Ha, T.D. Minh, H.M. Nguyet, A.K. Sharma, Ampicillin adsorption onto amine-functionalized magnetic graphene oxide: synthesis, characterization and removal mechanism, *Korean J. Chem. Eng.* 38 (2021) 22–31.
- [55] N. Rahman, P. Varshney, Assessment of ampicillin removal efficiency from aqueous solution by polydopamine/zirconium (IV) iodate: optimization by response surface methodology, *RSC Adv.* 10 (2020) 20322–20337.
- [56] J. Rösgen, Molecular basis of osmolyte effects on protein and metabolites, *Methods Enzymol.* 428 (2007) 459–486.
- [57] K.H. Hopmann, F. Himo, **Quantum chemical modeling of enzymatic reactions-applications to epoxide-transforming enzymes**, (2010).
- [58] A. Renita, P. Kumar, L. Abraham, Adsorption of ciprofloxacin from aqueous solution using surface improved tamarind shell as an economical and effective adsorbent, *Int. J. Phytorem.* (2021) 1–11.
- [59] A. Miri-Jahromi, M. Didandeh, S. Shekarsokhan, Capability of MXene 2D material as an amoxicillin, ampicillin, and cloxacillin adsorbent in wastewater, *J. Mol. Liq.* 351 (2022), 118545.